Linear array of complementary metal oxide semiconductor double-pass metal micromirrors

Johannes Bühler
Franz-Peter Steiner
ETH Zürich
Physical Electronics Laboratory
HPT H6
CH-8093 Zürich, Switzerland
mail: buehler@iqe.phys.ethz.ch

Roland Hauert
Swiss Federal Laboratories for Materials Testing and Research (EMPA)
Ueberlandstrasse 129
CH-8600 Dübendorf, Switzerland

Henry Baltes
ETH Zürich
Physical Electronics Laboratory
HPT H6
CH-8093 Zürich, Switzerland

Abstract. Low-cost linear arrays of deflectable micromirrors using a CMOS-compatible process to define both on-chip circuitry and the mirror structure are presented. The mirrors consist of the CMOS second metal layer deposited in two successive passes in order to establish a thick metal layer for the stiff mirror plate as well as a thin one for the flexible hinges. The mirrors are released by sacrificial aluminum and oxide etching. Supercritical point drying is performed in order to avoid sticking of the mirrors to the substrate. The mirrors are electrostatically deflected by biasing the address electrodes implanted into the substrate underneath the mirror plate. Full angular deflection by ±4.8 deg of a 30 × 40-μm^2 plate is achieved with a driving voltage of 11 V. On-chip circuitry adjacent to each mirror allows one to address the pixels with 5-V data pulses. The reflectance of the aluminum surface for wavelengths between 400 and 700 nm was measured to be 83% to 89%. The mirror surface was further characterized using Auger spectroscopy, showing that no optically relevant surface modifications occur during postprocessing. The surface rms roughness measured by atomic force microscopy is on the order of 25 nm.
[S0091-3286(97)00805-2]

Subject terms: micro-opto-electro-mechanical systems; deformable micromirror; torsional micromirror; micromirror array; spatial light modulator; surface micromachining; double-pass metal.

Paper MEM-08 received Nov. 6, 1996; revised manuscript received Jan. 8, 1997; accepted for publication Jan. 16, 1997.

1 Introduction

Linear arrays of deflectable micromirrors are of substantial interest as light modulators in printers and scanning devices. The integration of micromechanical and electronic devices on a single chip is indispensable in order to achieve large arrays with individually addressable pixels. Previously, electrostatically driven torsional mirror arrays were demonstrated using specific actuator processes,[1–3] some of them on top of a CMOS process. Others[4–6] introduce additional layers, such as polysilicon, for purely mechanical purposes into the standard process. In the case of polysilicon, however, the additional thermal budget from the deposition and annealing has to be considered for the fabrication of the electronic devices.

The contrast ratio of micromirror arrays is limited by the filling factor of the pixels, i.e., the mirror-to-mirror spacing divided by the pixel size. In applications using linear arrays, the optically relevant (active) area is a narrow line masking off the adjacent space where the optically inactive components of the light modulator can be placed. Consequently, the electronic components of each pixel and the etch holes can be designed adjacent to the mirror structure and do not have to be integrated into the area of the pixel. Therefore, the high level of process integration of conventional 2-D micromirror arrays is not required for a linear array, and a more efficient fabrication process is gaining interest.

A low-cost mirror fabrication needs to be based on a process as close to the standard IC process as possible with a minimum number of additional masks and process steps required. Mirror arrays can be fabricated at low cost when the IC process layers can be used for multiple purposes: to build up the mirror structure and the sacrificial layers that allow to release the mirror, as well as to fabricate the on-chip circuitry. In our approach, the most critical and expensive fabrication steps — layer deposition and patterning — are all done within the cost-effective IC process, and the postprocessing only consists of a low-cost, sacrificial-layer wet etching sequence to release the mirrors. The individual layer thicknesses required for the flexible as well as for the stiff parts of the mechanical device are obtained by depositing and patterning the mirror material in two passes as described in Sec. 2.

Aluminum is commonly available in standard processes as interconnect metal and shows a high optical reflectance. It is thus the favorite micromirror material. However, the progress in IC technology led to an optimization in the electrical but not necessarily in the optical properties of aluminum metallizations. Therefore, the surface characteristics and optical properties of various aluminum metallizations to be used in our devices were investigated (Sec. 3), and the results are discussed in Sec. 4.

2 Device Fabrication

The electrostatically actuated torsional micromirror consists of a stiff, free-standing mirror plate suspended from

The mirror plate acts as the upper electrode, and $n+$ implants within the $p-$epitaxial silicon located below each mirror wing serve as individually driven lower address electrodes (Fig. 1). Landing electrodes implanted the same way underneath the free edges of the mirror prevent it from sticking when the plate touches the substrate in the fully deflected state. Metal 1 and the intermetal (via) silicon dioxide are used as sacrificial layers and define the gap between the mirror and the lower electrodes. For good optical properties, good planarity of the mirror plate is essential, which is achieved by implanting the lower electrodes and thus avoiding any topographical step underneath the mirror.

The micromirror array and integrated on-chip circuitry were fabricated using the 1.6-μm double-metal CMOS process (called DIMOS01) at Delft University of Technology, The Netherlands. The process flow (Fig. 2) included the double-pass metal 2, a top photoresist layer instead of the silicon nitride passivation to protect the bonding pads and actuators during the postprocessing, and the dicing of the wafers.

The postprocessing consists of an etch sequence (Fig. 3) to release the actuators with no photolithographic step required:

1. The metal 1 sacrificial layer is wet-etched in a standard aluminum etch solution to undercut the structure in large lateral dimensions with high selectivity over the dielectrics and photoresist protecting the aluminum actuator.
2. The 1-μm-thick intermetal silicon dioxide protection is removed by a dip in Pad-etch for typically 16 min. Pad-etch is an ammonium fluoride etchant of sufficient selectivity to aluminum consisting of 13.5 wt% NH_4F, 31.8 wt% acetic acid, 4.2 wt% ethylene glycole, and water.[8] The samples are then rinsed for 10 s in deionized (DI) water.
3. In order to ensure a high processing yield, the natural oxide on top of the aluminum surfaces is enhanced by immersing the chips in a wet chemical oxidant after the pad-etch step. A period of 10 min in chromic acid or 30 min in hydrogen peroxide is sufficient to prevent the aluminum from being chemically attacked by the subsequent thorough rinse in DI water.
4. The top photoresist passivation is removed by acetone (2 min) and a final rinse in DI water.
5. Supercritical point drying using CO_2 in a commercial Baltec CPD030 system prevents sticking of mirrors to the substrate due to adhesion during drying. Acetone is used as the intermediate liquid between deionized water and the liquid CO_2.

Linear arrays of 16 pixels were integrated with an inverter next to the mirror to drive each pixel individually (Fig. 4). The size of the mirror plate and the air gap between mirror and lower electrodes were chosen to be 30×40 μm^2 and 1.7 μm, respectively, resulting in a maximum mirror deflection of ±4.8 deg. The mirror suspensions were 0.3 μm thick, 15 μm long, and 2.4 μm wide, setting the threshold voltage for the full deflection to 11 V.

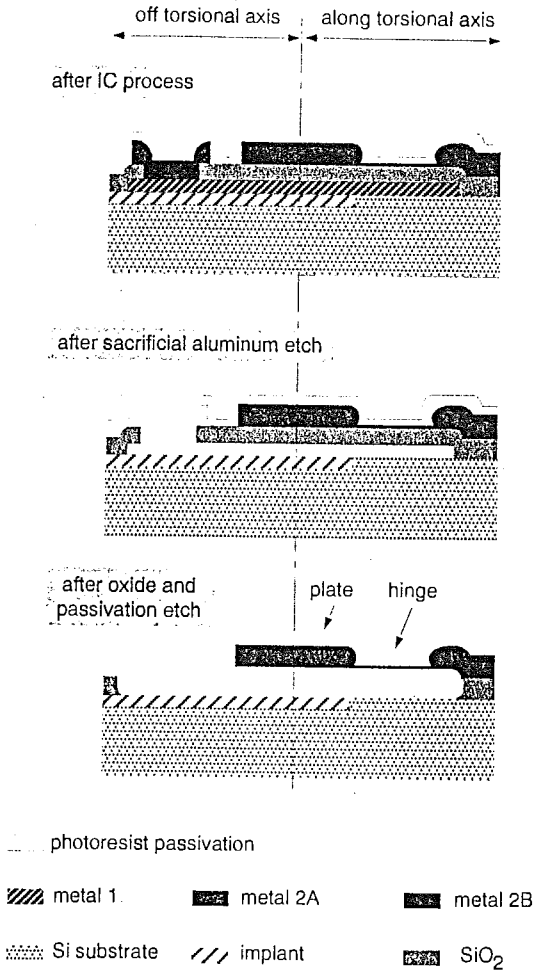

Fig. 3 Schematic cross section of the mirror plate and the mirror hinges after the CMOS process and the postprocessing sacrificial-layer etch steps.

3 Mirror Surface Characterization

In order to qualify the aluminum mirror layer available from the IC process for optical applications and to investigate the surface modifications induced by the postprocessing etch sequence, we measured the surface roughness, the thickness of the native oxide formed on top of the Al-1%Si layer, and the optical reflectance as a function of the wavelength of incident light, each before and after the postprocessing steps.

The surface rms roughness of aluminum test layers was determined from the surface profile taken by atomic force microscopy (AFM). Four sample wafers were prepared, each coated with different aluminum layers sputter-deposited on top of the plasma-enhanced CVD (PECVD) silicon dioxide used as intermetal oxide in the CMOS process: Al-1%Si at a thickness of 0.9 μm at 250 °C sputter temperature (No. 1), 0.3 μm sputtered as close to room temperature as possible (No. 2), 0.3 + 0.6 μm (double-pass

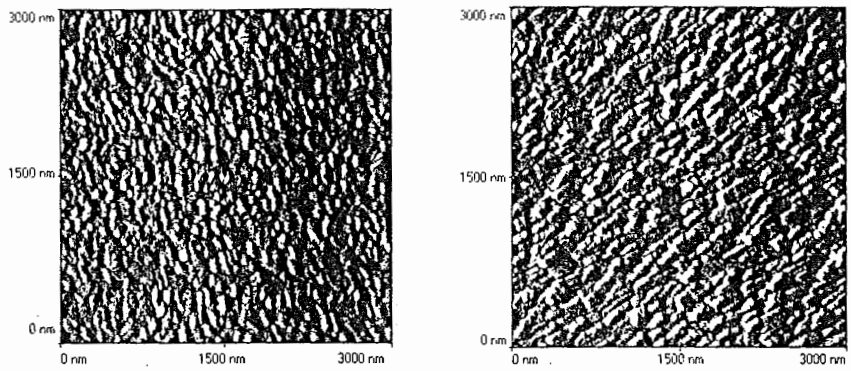

Fig. 6 Atomic force micrographs of test metallizations sputter-deposited in two subsequent passes of 0.3- and 0.6-μm thickness at room temperature. The film surface as deposited (a) differs only slightly from the surface after the passivation lithography and postprocessing sequence (b).

the test aluminum surface sputter-deposited in two subsequent passes of 0.3- and 0.6-μm thickness at room temperature is compared before and after postprocessing in order to evaluate the influence of the photolithography and etching procedure on the optical properties.

Within the range of visible light, a sufficiently flat spectrum with a maximum reflectance of 88.5% was obtained, decreasing below 84% in the UV and near-infrared regimes. A reflectance enhanced by 1% in the visible range was obtained for a thin aluminum layer of 0.3-μm thickness, also sputtered at room temperature. The aluminum is highly reflective above a wavelength of 1000 nm. This reflectance behavior agrees with literature data for metallic aluminum with surface and, possibly, even bulk oxidation of the samples.[10] Note that the reflectance of aluminum even under ultrahigh-vacuum deposition conditions[10] does not exceed maximum values of 93%. The postprocessing results in a reflectance lowered by not more than 2% in the visible and an insignificant change for $\lambda > 850$ nm.

In order to further investigate if the decreased reflectance could possibly be related to an increased layer thickness of native aluminum oxide on top of the samples, scanning Auger spectroscopy[11] was performed. Two samples were compared to determine the influence of the postprocessing on the aluminum films (sputter-deposited at room temperature): aluminum as deposited and after postprocessing. Their differentiated Auger spectra are shown in Fig. 8. The metallic aluminum peaks (*KLL* and *LMM*) and the oxygen of the native oxide are comparable, but a significant carbon contamination is found on the postprocessed surface.

The samples were then sputter-etched *in situ* and the Auger spectrum was taken after every 10 s of sputter time. With the etchback of the film, a depth profile of the relative aluminum, oxygen, and carbon content is obtained (Fig. 9). The surface depth is calculated for each material using the etch rates given in Table 2.

For the postprocessed sample, the oxygen distribution and, accordingly, the metallic aluminum concentration develop deeper into the film, but the corresponding native aluminum passivation grew in thickness by not more than 0.8 nm during postprocessing. The carbon contamination was 1 to 4 monolayers thick and likely originated from the photolithographic step during the postprocessing sequence. This slightly increased passivation of aluminum can possibly explain the decreased reflectance described above.

Table 1 Deposition and film properties of the samples characterized by atomic force microscopy.

Sample no.	Layer thickness (μm)	Deposition temperature (°C)	σ_{rms} (nm)	Intrinsic stress (MPa)
1	0.9	250	53±5	+250
2	0.3	≈20	12.5±1	−50
3	0.3±0.6	≈20	21±2	+60
4	0.3±0.6	≈20	25±3	+60

4 Results and Discussion

The performance of the individual micromirrors was tested by measuring the angular deflection versus driving voltage. Using a UBM confocal microscope, the deflection height is measured at two points of known distance on top of the mirror surface, from which the angular deflection is calculated. The result in Fig. 10 shows a threshold voltage V_{th} of 10.8 V for the full mirror deflection of 4.8 deg, in good agreement with the theoretical value of 11.7 V calculated from linear elasticity theory and a simplified geometry of the lower electrodes.

In order to demonstrate the CMOS compatibility of the double-pass metal actuator, a CMOS inverter is placed next to each pixel of the linear array (Fig. 4) to drive the individual mirrors and the corresponding landing electrodes. The inverter can be switched with *S-V* data pulses. The two address electrodes underneath the mirror "wings" are connected to a constant voltage larger than V_{th} and OV,

Table 2 Etch rates and thickness of the aluminum passivation layers obtained by Auger spectroscopy.

Material	Etch rate (nm/min)	Thickness (nm)	
		Before postprocessing	After postprocessing
Al (met.)	20	-	-
Al_2O_3	6	2.4	2.4–3.2
C	3	Not significantly present	0.4–1.2

plates and rectangular torsional hinges.[12] Depending on the optical application, a torsional axis diagonal with respect to the row of the mirrors[1] may be preferred to a perpendicular axis of rotation.

5 Conclusions

It was shown that linear arrays of torsional micromirrors can be fabricated at low cost and integrated with on-chip circuitry using a CMOS process with double pass metallization.

Due to their high reflectance, CMOS Al-1%Si layers are well suited for optical applications, and the smoothness of the surface is enhanced when the sputter temperature is reduced as much as the required step coverage allows. The postprocessing steps to release the aluminum actuator do not significantly degrade the optical properties of the aluminum surface: the passivation film on top of the metallic aluminum increases by not more than approximately 1 nm, and the absolute reflectance is lowered by a maximum of 2% to values between 83% and 89% in the spectral range of visible light. Consequently, the postprocessing is compatible with optical devices.

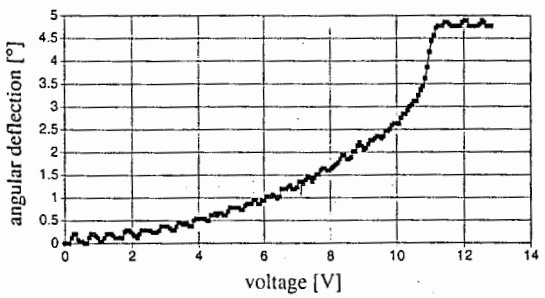

Fig. 10 Angular deflection versus driving voltage biasing the address electrode of the torsional mirrors shown in Fig. 4.

Acknowledgments

The authors are indebted to P. M. Sarro and H. Schellevis, DIMES, Delft University of Technology for their work on implementing the double-pass metal process and for providing the CMOS and aluminum test film samples. We also thank L. Eng and M. Abplanalp for the atomic force micrographs. The reflectance measurements performed by GRETAG AG, Regensdorf, are gratefully acknowledged. E. Bolz contributed to the choice of the etch chemistry with some valuable discussions. This work was funded by the Swiss Federal Priority Program LESIT.

References

1. L. J. Hornbeck, "Digital light processing and MEMS: timely convergence for a bright future." *Proc. SPIE* **2642**, 2 (1995); preprint available from Texas Instruments, Dallas, Texas.
2. C. W. Storment, D. A. Borkholder, V. Westerlind, J. W. Suh, N. I. Maluf, and G. T. A. Kovacs, "Flexible, dry-released process for aluminum electrostatic actuators," *J. Microelectromech. Syst.* **3**(3), 90–96 (1994).
3. K. E. Mattson, "Surface micromachined scanning mirrors," *Microelectronic Eng.* **19**, 199–204 (1992).
4. V. P. Jaecklin, C. Linder, N. F. de Rooij, J.-M. Moret, and R. Vuilleumier, "Line-addressable torsional micromirrors for light modulator arrays," *Sensors and Actuators A* **41–42**, 324–329 (1994).
5. N. C. Tien, O. Solgaard, M.-H. Kiang, M. Daneman, K. Y. Lau, and R. S. Muller, "Surface-micromachined mirrors for laser-beam positioning," in *Digest of Technical Papers, The 8th International Conf. on Solid-State Sensors and Actuators (Transducers '95)*, Vol. 2, pp. 352–355, Stockholm, Sweden (1995).
6. M. B. Fischer, H. Graef, and W. von Münch, "Electrostatically deflectable polysilicon torsional mirrors," *Sensors and Actuators A* **44**, 83–89 (1994).
7. J. Bühler, J. Funk, F.-P. Steiner, P. M. Sarro, and H. Baltes, "Double pass metallization for CMOS aluminum actuators," in *Digest of Technical Papers, The 8th International Conf. on Solid State Sensors and Actuators (Transducers '95)*, Vol. 2, pp. 360–363, Stockholm, Sweden (1995).
8. Etchant No. 17668, Riedel-deHäen, Seelze, Germany (1995).
9. P. A. Flinn, "Principles and applications of wafer curvature techniques for stress measurements in thin films," *Mat. Res. Soc. Symp. Proc.* **130**, 41–50 (1989).
10. D. Y. Smith, E. Shiles, and M. Inokuti, "The optical properties of metallic aluminum," in *Handbook of Optical Constants of Solids*, pp. 369–406, Academic Press, Orlando (1985).
11. S. Hofmann, in *Practical Surface Analysis*, D. Briggs and M. P. Seah, Eds., pp. 143–194, Wiley, New York (1990).
12. J. Funk, J. G. Korvink, M. Bächtold, J. Bühler, and H. Baltes, "Coupled 3D thermo-electro-mechanical simulations of microactuators," in *Proc. IEEE Workshop on Microelectromechanical Systems*, pp. 133–138, San Diego, CA (1996).

Johannes Bühler received the diploma degree in physics from the University of Karlsruhe, Germany, in 1992. He is currently pursuing the PhD. degree at the Swiss Federal Institute of Technology (ETH) in Zurich. His research activities include the design, fabrication, and characterization of thermal and electrostatic microactuators.

Franz-Peter Steiner received his diploma in physics and his PhD from the Swiss Federal Institute of Technology (ETH Zurich) in 1985 and 1990, respectively. After several years in industry, last as manager of a product line of semiconductor process equipment, he returned to ETH as a program and project leader. His research interests include design and simulation of microelectromechanical systems. He is head of the microactuators and the chemical sensors group and deputy director of the Swiss priority